IEEE Access
Multidisciplinary | Rapid Review | Open Access Journal

Received October 1, 2020, accepted November 5, 2020, date of publication November 9, 2020, date of current version November 19, 2020.

Digital Object Identifier 10.1109/ACCESS.2020.3036886

A T-Type Self-Decoupled and Passive Dynamic Tension and Torque Sensor: Design, Fabrication, and Experiments

YISONG TAN, (Member, IEEE), YIFU FU, XINYU WANG, MOYUE CONG, AND LIMIN REN, (Member, IEEE)
School of Mechanical Engineering, Northeast Electric Power University, Jilin City 132012, China

Corresponding author: Limin Ren (renlimin@neepu.edu.cn)

This work was supported in part by the Key Projects of Science and Technology Development Plan of Jilin Province under Grant 20190201103JC, in part by the Science and Technology Program of the Education Department of Jilin Province under Grant JJKH20200103KJ, and in part by the Science and Technology Program of Jilin City under Grant 20190104208 and Grant 20200104115.

ABSTRACT Self-decoupled and passive characteristics are crucial requirements for a multi-dimensional sensor. A T-type self-decoupled and passive dynamic tension and torque sensor was proposed, analyzed, and fabricated. The sensor mainly consisted of a T-type torque deforming block, a force deforming ring, and a torque shaft. The T-type torque deforming block withstood the torque individually; the force deforming ring bore the tension force separately; and the decoupling of the tension force and torque was realized by the torque shaft. After that, the tension force and torque were measured, respectively. The decoupling operation was fully completed by mechanical structure. Two pieces of magnetostrictive material were pasted on the T-type torque deforming block and force deforming ring as the sensing units. The passive feature was fulfilled by the magnetostrictive material via the Villari effect. Finite Element Method (FEM) analysis was carried out to verify the decoupling principle. The sensor was fabricated, and then the experiments were conducted. The results showed that the sensor had a good decoupling ability. The sensor could work dynamically with a voltage deviation less than 0.5 mV. The force and torque ranges of the sensor were 1000 N and 6.5 N·m respectively. The sensor could also work effectively in a passive state. Furthermore, the sensor displayed the advantages of being wireless, the ability to work dynamically and in a liquid environment. Thus, this sensor could be mounted on a cutting tool of a machine center to detect the compound force on the cutting tool.

INDEX TERMS Self-decoupled, passive, tension force, torque, working in liquid.

I. INTRODUCTION

Multi-dimensional sensors have gained great achievements in the field of robots, precision manufacturing, and machine centers [1]–[6]. Liang *et al.* proposed a five-dimensional force/torque sensor based on strain gauges and cross beams [7]. Most of the existing multi-dimensional sensors are based on the Maltese cross beam structure [8] or the Stewart structure [9]. Some of the multi-dimensional sensors are also based on the deformed structure of the Maltese cross beam or the Stewart structure [10], [11]. The multi-dimensional sensor is subject to compound force, torque, and moment at the same time, and the existing multi-dimensional sensors use an additional calibration matrix to indirectly decouple the compound force [12], [13]. Special algorithms are needed in these sensors to give out the individual force component. The decoupling operation leads to some problems such as complication, or not visibly expressing each individual component [14]. It brings great benefits for designing the sensor and understanding the actual force applied on the multi-dimensional sensor if every output can directly express every individual force component.

The power supply and the ability of the multi-dimensional sensor to rotate a full circle are also crucial problems in practical industrial application [15]–[17]. The main sensing material used in existing multi-dimensional sensors are piezoresistive material [7], optical grating [18], [19], and piezoelectric material [20]. The power supply and signal transmission of these three kinds of materials are all via electric wires. The wires hinder the sensor from rotating a full

The associate editor coordinating the review of this manuscript and approving it for publication was Jenny Mahoney.

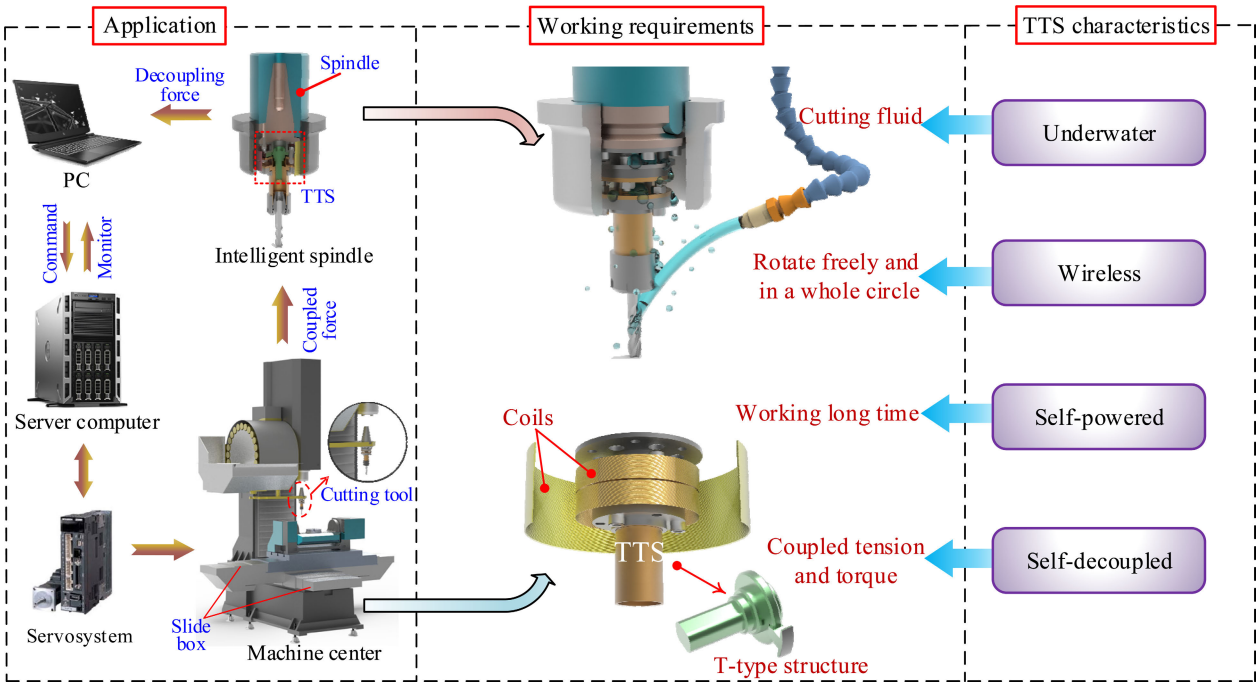

FIGURE 1. Framework and application of the self-decoupled and passive dynamic tension and torque sensor (TTS).

circle, and the wires also block the sensor from being used in a dynamic environment. Although some multi-dimensional sensors use batteries to supply power to these materials, the energy stored in the battery is limited [21]. The sensor must stop working to replace the exhausted battery; under this situation, the sensor cannot work for a long or unlimited time [15], [22]. The power supply problem, and the wireless problem can be regarded as one unified passive problem in the design and application of multi-dimensional sensors. If a multi-dimensional sensor can fulfill the passive feature, it will be beneficial.

Some working environments, such as a machine center, are harsh. The multi-dimensional sensor must withstand a severe cutting liquid environment [21]. The existing piezoresistive material, optical grating, or piezoelectric material cannot be directly applied in such environment. Special measures must be taken to protect the sensing materials. Therefore, working in liquid environment is also a fundamental requirement for a multi-dimensional sensor.

To sum up, being self-decoupled and passive, and being able to work dynamically and in a liquid environment are comprehensive requirements for a multi-dimensional sensor. In this article, we propose a T-type self-decoupled and passive dynamic tension and torque sensor (TTS). In contrast to previous works, the TTS can decouple the tension force and torque directly without any additional algorithm. The TTS can work passively and wirelessly without any onboard batteries or wires on them, and it can also work normally in a liquid environment.

The problem formulation, materials, design, mechanism, fabrication, and experiment are presented in Section II. Section III describes the experiment results in detail. Section IV is the discussion section, and conclusions are drawn in Section V.

II. MATERIALS AND METHODS

A. PROBLEM FORMULATION

The purpose of this study was to present a self-decoupled and passive dynamic tension and torque sensor. The proposed TTS can be mounted directly on the upper end of a cutting tool, which is a crucial component of the machine center, as shown in Fig.1. The information of the cutting tool is prominent for industrial fabrication and manufacturing processes. It can also provide fundamental elements to the "Industrial Internet" through server computer. The cutting tools is subject to vigorous working conditions, including a compound tension force and torque, working for a long time, rotating freely and in a whole circle, and being embraced by cutting fluid. The compound force and torque are induced by the feeding movement of the cutting tool and slide box. Working for a long time means that the movement of the cutting tools cannot be disrupted, and rotating freely and in a whole circle means the sensor cannot hinder the cutting tool from rotating. Meanwhile, being embraced by cutting fluid means that the sensor must have the ability to work appropriately in a liquid environment.

Referring to these vigorous demands listed above, the TTS is proposed in the paper. The decoupling operation is accomplished by a special designed T-type structure, which is much different to the existing decoupling method. The force sensing operation is fulfilled by a smart magnetostrictive material. The characteristics of being passive and being wireless

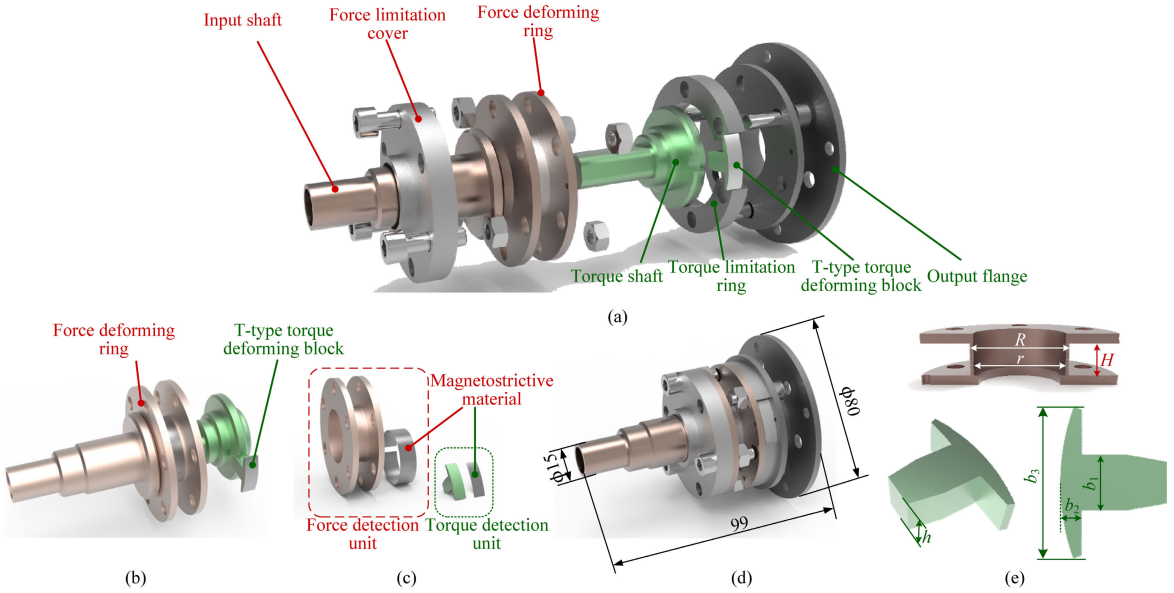

FIGURE 2. View and structure of the TTS. (a) explosion view of the TTS; (b) key force detecting component; (c) detecting units; (d) axonometric projection;(e) parameters of the force deforming parts, $R = 15$mm, $r = 14$mm, $H = 10$mm, $b_1 = 7.05$mm, $b_2 = 2.59$mm, $b_3 = 19.15$mm, $h = 6$mm.

are also realized by the sensing material. The underwater ability is achieved by the combination of the magnetostrictive material and a specially designed detecting system. The detailed design and verification of the TTS will be illustrated one-by-one in the following parts.

B. FORCE SENSING MATERIAL

The force sensing material used in the TTS is a magnetostrictive material (Metglas 2826MB, SC, USA), which contains 40% Fe, 38% Ni, 4% Mo, and 18% B ($Fe_{40}Ni_{38}Mo_4B_{18}$). The 2826MB magnetostrictive material is known as an amorphous ferromagnetic ribbon, which has a thickness of only 28 μm and a high magnetostrictive coefficient of up to 11.7 ppm [23]. The amorphous ribbon makes the force sensing operation feasible in all directions, just the opposite of the crystal magnetostrictive material. The 28 μm ultra-thin thickness of the 2826MB brings no mechanical influences to the TTS. The high magnetostrictive coefficient means that the sensing material is more sensitive to external applied force, for more magnetic permeability change is realized under the same stress. All of the merits above make the 2826MB more suitable for force sensing purposes than Terfenol-D and Galfenol [24].

C. STRUCTURE OF THE TTS

Fig.2 shows the structure of the TTS, which consists of an input shaft on the left and an output flange on the right. The input shaft is used for importing the coupled dynamic tension and torque, and the output flange is to export the decoupled tension and torque. The overall dimensions of the sensor are 80 mm in its maximum output flange diameter, 15 mm in its minimum input shaft diameter, and 99 mm in its total length, as shown in Fig.2(d). Fig.2(a), (b) and (c) show the explosion view of the TTS, which gives a clear view of the internal structure of the TTS. The force limitation cover and the force deforming ring are assembled after the input shaft. A piece of magnetostrictive material is pasted on the force deforming ring to detect the tension force. The torque shaft, the torque limitation ring, and the T-type torque deforming block are installed before the output flange. The other piece of magnetostrictive material is stuck on the T-type torque deforming block to detect the torque. Fig.2(d) gives the exact parameters of the force and torque deforming parts of the TTS.

D. OPERATING MECHANISM

The operating mechanism of the TTS is given in Fig.3. A compound input, including a tension force F_0 and a torque T_0, acts on the input shaft. The linear movement induced by the tension force F_0 and the rotation movement induced by the torque T_0 are separated by the special configuration of the torque shaft, as shown in Fig.3(b). Due to the linear movement along the torque shaft, the energy of the tension force F_0 propagates along the blue dotted line, as shown in Fig.3(a).

Note that there is no tension force acting on the torque shaft or the torque limitation ring at all, which means that the force has no influence on the torque detecting components due to the special structure of the TTS. On the other hand, as shown in Fig.3(c), the energy of the torque T_0 propagates along the input shaft, the torque shaft, the torque limitation ring, and the T-type block, shown in pink dotted line.

It is also noted that there is no additional torque acting on the force detecting components of the TTS. Through the special structure of the proposed sensor, the compound F_0 and T_0 are measured by two individual components of the

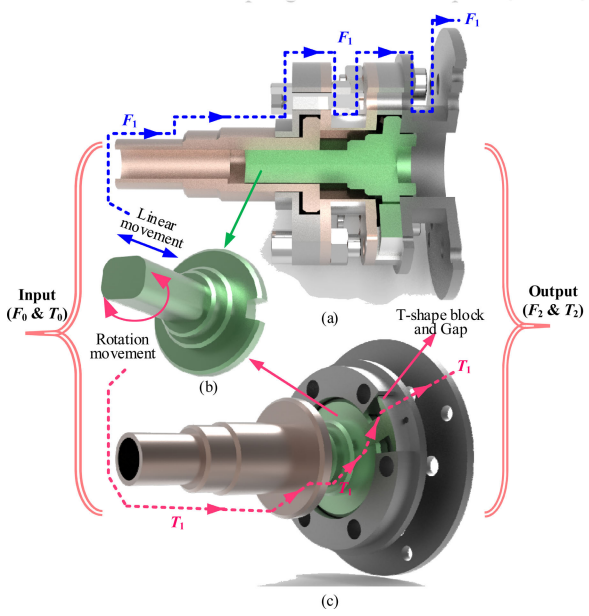

FIGURE 3. Mechanical operating mechanism of the TTS. (a) tension force transmission flow; (b) torque shaft; (c) torque transmission flow.

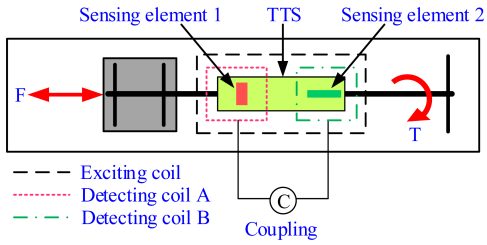

FIGURE 4. Arrangement of the exciting coil and their corresponding detecting coils. F and T are force and torque acting on the TTS respectively.

sensor. No interference exists between the two components, which realizes self-decoupling between the input F_0 and T_0.

The detecting principle of the force and torque is based on the Villari effect [23]. Two pieces of magnetostrictive material are pasted on the sensitive regions of the force and torque deforming components, as shown in Fig.2. When subjected to tension force and torque, external stresses are applied on these two magnetostrictive materials. The permeability of these two ribbons change due to the Villari effect under an external magnetic field. The changed permeabilities lead to variations of the spatial magnetic flux density. The changed spatial magnetic flux densities are captured finally by two detecting coils arranged at the force and torque sensitive regions according to Faraday's law of electromagnetic induction. The arrangement of the two coils and their corresponding magnetostrictive material are illustrated in Fig.4. The induced voltages in the two coils are dependent on the stress caused ty the tension force and torque. That is to say, the induced voltage can individually reflect the external tension force and torque.

E. FINITE ELEMENT METHOD ANALYSIS

In order to verify the self-decoupled performance of the TTS, an Finite Element Method (FEM) analysis was conducted, as shown in Fig.5. The material of the TTS is 7075 aviation aluminum with a mass density of 2700 kg/m^3. The meshing method and size of the TTS are Solid 186 and 0.10, respectively.

In Fig.5(a), an individual tension force of 500 N is applied on the TTS. There is an obvious strain in the force deforming ring, the value of which is 2.316×10^{-3}. Meanwhile, the strain on the T-type torque deforming block is almost equal to 0, which means that the tension force has no influence on the torque detection. In Fig.5(b), an individual torque of 5 N·m is applied on the TTS separately. Similar to Fig.5(a), an obvious strain appears in the T-type torque deforming block, the value of which is 1.950×10^{-3}; however, there is almost no strain in the force deforming ring. In Fig.5(c), a combined tension force (500 N) and torque (5 N·m) are applied on the TTS at the same time. Two main strains occur at the force deforming ring and the T-type torque deforming block, respectively, the values (2.293×10^{-3} and 1.637×10^{-3}) of which are also equal to those under individual force and torque.

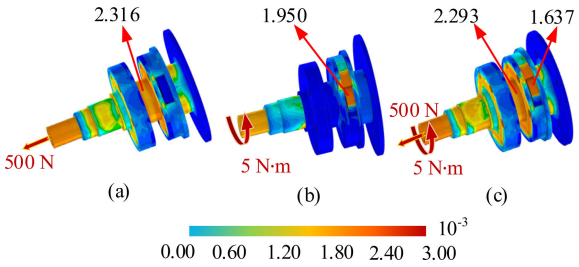

FIGURE 5. FEM results: (a) tension only; (b) torque only; (c) combined tension and torque.

Fig.5(a), (b) indicate that the TTS can effectively reflect the tension force and torque, while Fig.5(c) indicates that there is no cross-disturbance between the tension force input and torque input. The FEM analysis results in Fig.5 comprehensively demonstrate the self-decoupled ability of TTS. The FEM analysis results also tell us the most appropriate position to paste the magnetostrictive material, which is also the second purpose for conducting the FEM analysis.

F. PROTOTYPE OF THE TTS

A prototype of the TTS was fabricated to verify the design of the TTS, as shown in Fig.6. The TTS is made of 7075 aviation aluminum after a surface-anodized treatment. It has a length of 99 mm and a weight of 375 g.

G. THE EXPERIMENT SETUP

A dynamic test platform was designed and developed to verify the self-decoupled characteristics and dynamic performance of the TTS, as shown in Fig.7.

Fig.7(a) shows the mechanical system of the dynamic test platform. The whole length and height of the test platform are 2400 mm and 1200 mm, respectively. A servo motor is arranged on the left to provide a dynamic rotating velocity. The rotating velocity can be acquired by a self-developed

FIGURE 6. The prototype of the TTS.

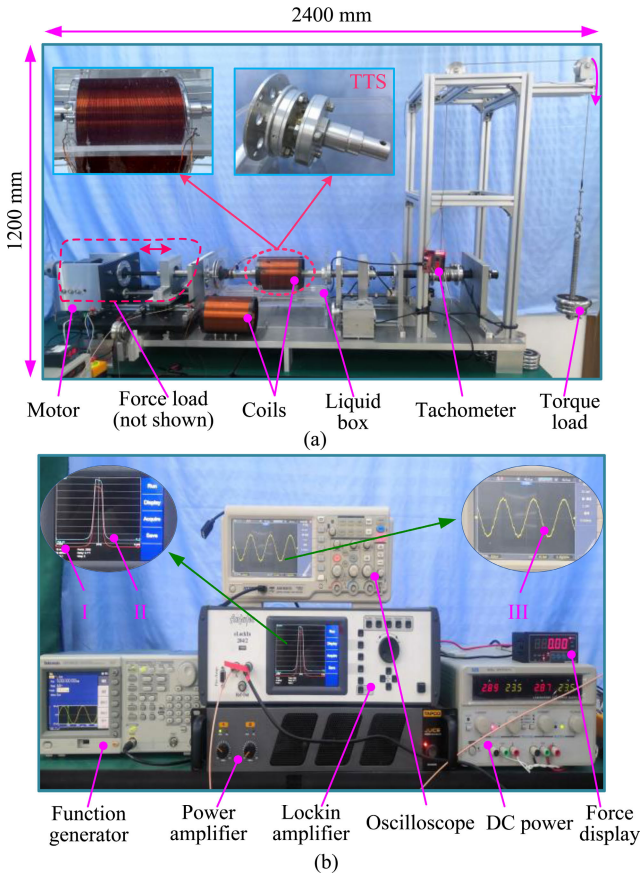

FIGURE 7. The experimental setup of the TTS: (a) mechanical system; (b) electronic system. (I) and (II) refer to the signals of the tension force and torque in the frequency domain, (III) is the signal in the time domain.

tachometer on the right. The tension force load is applied by a handwheel under the servo motor and transmitted by a trapezoidal screw. The value of the tension force is obtained by a force load cell on the right. The handwheel, the trapezoidal screw, and the force load cell are all shown in the Fig.7(a). The torque load is applied by different weights through two pulleys. The TTS is placed inside three coils (one exciting coil and two detecting coils), the exact physical dimensions of which are given in Table 1. The TTS, together with the three coils, was immersed in a liquid box to provide a liquid environment.

TABLE 1. Physical dimensions of the three coils.

Coils	Copper wire	Turns	Diameter	Length
Exciting coil	Line 23 (0.6 mm)	305	150 mm	168 mm
Detecting coil 1	Line 29 (0.3 mm)	290	90 mm	20 mm
Detecting coil 2	Line 29 (0.3 mm)	290	90 mm	20 mm

Fig.7(b) shows the electronic system of the test platform. A function generator (Tektronix AFG 3021C, Oregon, USA) exports a sinusoidal signal with a frequency of 5000 Hz and an amplitude of 2 mV. The sinusoidal signal is input into a power amplifier (J.2500, Washington, USA). The amplified signal is then input into the exciting coil to get an exciting magnetic field. A lockin amplifier (E Lock In 204/2, Oelsnitz, German) is used to analyse the signals from the two detecting coils. It is noted that the lockin amplifier used in the test platform has two channels, and it can analyse the signals from the tension and torque deforming elements at the same time. One channel of the lockin amplifier is linked to the tension force detecting coil, and the other channel is linked to the torque detecting coil. (I) and (II) in Fig.7(b) refer to the signals of the tension force and torque in the frequency domain, while (III) is the signal in the time domain. The servo motor is driven by DC power (MPS3010LP-2, Shenzhen, China).

III. RESULTS

Fig.8 shows the plot of the voltage output versus an individual tension force. The signal was obtained from channel I of the lockin amplifier. The force was from −1000 to 1000 N, while the output voltage was from 83.33 to 84.67 mV. On the whole, the output voltage increased as the tension force increased. The entire force input could be divided into two regions: the compression region and the tensile region. It can be seen clearly that the voltages in the tensile region are larger than any one voltage in the compression region. This can be taken advantage of to determine the direction of the force. When the tension force was from −100 to 100 N, there was a voltage jump from 83.7 to 84.3 mV, which had a higher detection sensitivity and was more suitable for small tension force detection.

Fig.9 shows the plot of the voltage output versus an individual torque. The signal was obtained from channel II of the lockin amplifier. During the whole test, the range of the torque was (0, 7 N·m), while the voltage range was (93.2, 94.1 mV). In the whole torque range, the output voltage increased monotonously as the torque increased. There was a critical point, as observed in Fig.9, namely, torque 5.57 N·m and voltage 94.1 mV; before torque 5.57 N·m, the voltage increased until 94.1 mV, while after torque 5.57 N·m, the voltage did not increase, almost regardless of the amount the torque increased by. The reason for this phenomenon was that the 2826MB became saturated when the torque was over 5.57 N·m. Therefore, the detection range of the TTS can be determined according to this.

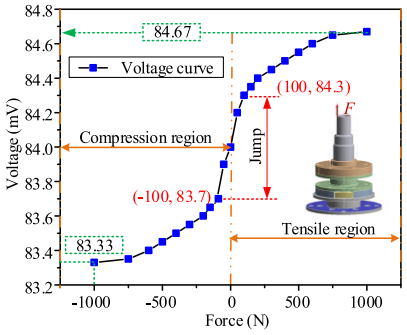

FIGURE 8. Plot of the voltage output versus an individual tension force.

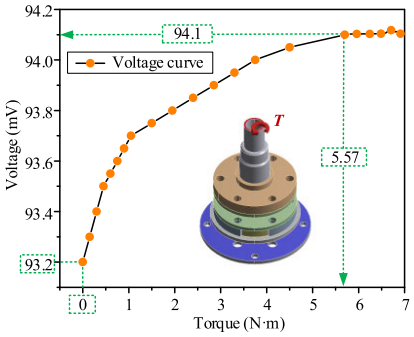

FIGURE 9. Plot of the voltage output versus an individual torque.

Fig.10 shows the voltage in the tension force detecting coil versus the applied tension force under different torques. The applied torques were 1.5 N·m, 3.0 N·m, and 4.5 N·m. The voltage–tension force curve under 0 torque can be seen as a standard curve. From Fig.10, it can be seen clearly there are no visible differences between the three curves and the standard curve (0 torque). Therefore, the torque has no influence on the voltage output of the tension force.

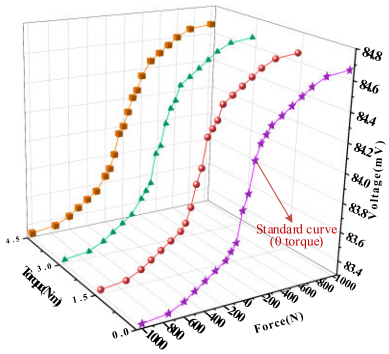

FIGURE 10. Plot of the voltage versus tension force under different torques.

Fig.11 reflects the plot of the voltage versus torque under different tension forces. The applied tension forces were 200 N, 300 N, and 400 N, respectively. The voltage–torque curve under 0 tension force can also be seen as the standard curve. From Fig. 11, the three curves under the tension force of 200 N, 300 N, and 400 N almost coincided with the standard curve. There are no obvious differences among these four curves, which indicates further that the tension force has no influence on the voltage output of the torque.

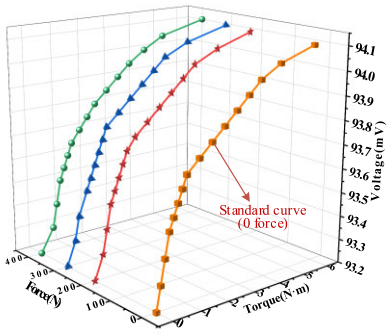

FIGURE 11. Plot of the voltage versus torque under different tension forces.

Fig.12 shows the plot of the voltage versus tension force under different rotating velocities. During the experiment, the TTS rotated at three different velocities, which were 20, 40, and 60 rpm, respectively. The three curves (20, 40, and 60 rpm) were almost the same as those when the rotating velocity was 0 rpm. Only a tiny difference existed when the tension force was around 100 N, at which the maximum voltage deviation was 0.02 mV. The 0.02 mV voltage deviation was much smaller than the entire voltage and did not alter the output of TTS. The reason for the maximum voltage deviation was the higher detection sensitivity in the jump area, as indicated in Fig.8.

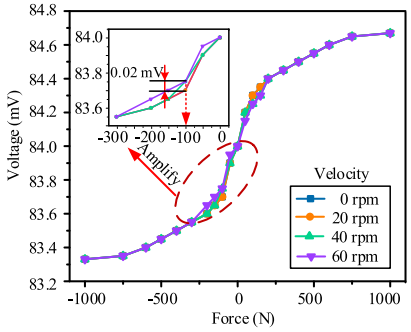

FIGURE 12. Plot of the voltage versus tension force under different rotating velocities.

Fig.13 shows the plot of the voltage versus torque under different rotating velocities. During the whole experiment, the TTS also rotated at three different velocities. The three curves coincided with the 0 rpm one. The maximum voltage deviation was 0.05 mV, which occurred at a torque of 0.9 N·m. The voltage deviation was very small and almost had no influence on the performance of the TTS. The above experiment results further indicate that the rotating velocity did not affect the performance of the TTS.

Fig.14 shows the drift characteristics of the TTS. The experiment lasted 3 days (72 h) and the voltages were recorded every 30 mins. In Fig.14(a), the voltages of

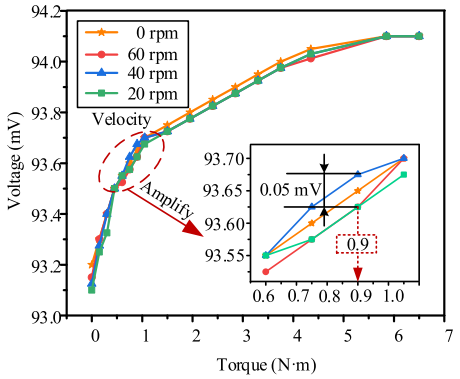

FIGURE 13. Plot of the voltage versus torque under different rotating velocities.

−1000 N, −400 N, −100 N, 0 N, 50 N, 200 N, and 600 N forces were recorded. During the 72-h test, there was no visible drift of these voltages during the whole test period. In Fig.14(b), torques of 0 N·m, 0.3 N·m, 1.0 N·m, 3.0 N·m, and 5.0 N·m were applied on the TTS separately for 72 h, and the voltages of the corresponding torque were recorded. No apparent difference could be seen during the whole experiment.

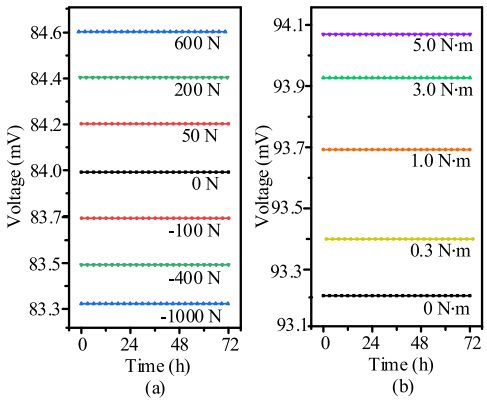

FIGURE 14. Drift characteristics of the TTS: (a) tension force voltage drift characteristic; (b) torque voltage drift characteristic.

Fig.15 reflects the hysteresis characteristics of the TTS. The tension force was applied forward and backward. In Fig. 15(a), the tension force increased from −1000 to 1000 N, and then decreased from 1000 to −1000 N. The voltage increased from 83.3 to 84.7 mV, and then decreased from 84.7 to 83.3 mV. The maximum deviation was 0.02 mV, which occurred at a force of 400 N. In Fig.15(b), the torque increased from 0 to 6.0 N·m, and then decreased from 6.0 to 0 N·m. The voltage increased from 93.2 to 94.1 mV, and then decreased from 94.1 to 93.2 mV. The maximum deviation was 0.05 mV, which occurred at a torque of 0.5 N·m.

In order to verify the working ability in a liquid environment of the TTS, a liquid dynamic working environment was constructed. Fig.16 shows the experimental process. In the experiment, the TTS was fully immersed in the water. Then, different tension forces and torques were applied on the TTS.

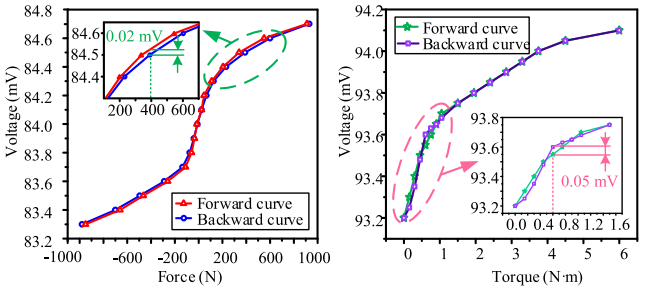

FIGURE 15. Hysteresis characteristics of the TTS: (a) plot of the forward and backward voltage output versus tension force; (b) plot of the forward and backward voltage output versus torque.

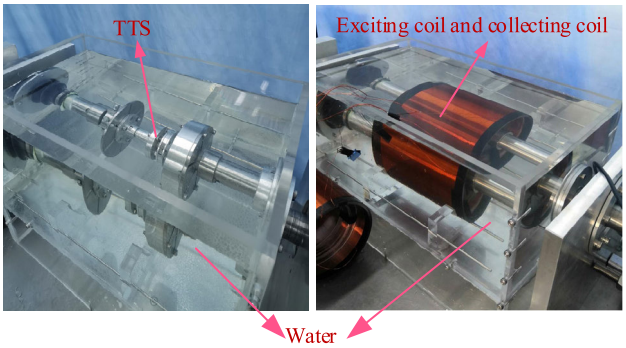

FIGURE 16. The TTS works in water.

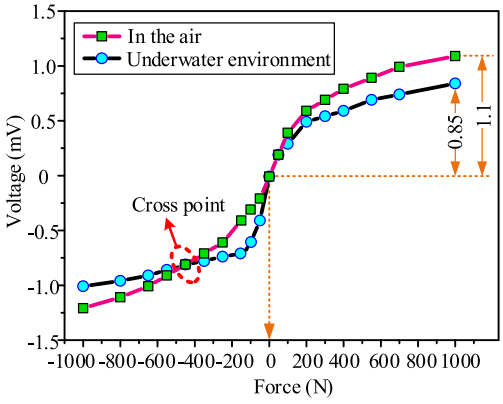

FIGURE 17. Output voltage comparison of the TTS in an air and a water environment.

Fig.17 shows the output voltage comparison of the TTS in an air and a water environment.

The voltage increased as the tension force increased. The curve in the air and the curve in the water had the same changing tendency; the only difference between the two curves was the voltage increment. The voltage increment in the air was 1.1 mV, and the voltage increment in the water was 0.85 mV, which means that the increment in the water was smaller than that in the air. The reason for the different increment will be given in the discussion part.

IV. DISCUSSION

Reflecting the actual force and torque accurately is a basic requirement for the TTS. This requirement is verified by Fig.8 and Fig.9. In Fig.8, the voltage increased as the tension

force increased synchronously. The TTS can reflect the tension force accurately. In Fig.9, the situation is similar, namely, the voltage in the torque detection coil can also reflect the torque accurately. Fig.8 and Fig.9 together prove the soundness of the TTS design.

In Fig.8, the state of the tension force changed from compressive force to tensile force. There was a voltage output jump from tension force −100 N to 100 N. The voltage in the tension region was larger than that in the compression region. The voltage output not only reflected the amplitude of the tension force, but also the direction of the tension force. This will be useful in practical applications, such as judging the feeding direction of the cutting tools of a machine center.

The force and torque ranges of the TTS are 1000 N and 6.5 N·m respectively in its present form, which are relatively small. The two ranges both can be increased by broadening the geometrical dimensions of the force deforming units or by replacing the aluminum with stainless steel. In terms of the force ranges, the external diameter R can be increased or the internal diameter r can be decreased to broaden the force ranges. In terms of the torque range, the width b_1, b_2, b_3 and h can be expanded to broaden the torque range. Further, by replacing the aluminum with stainless steel, the elastic modulus can be increased from 90 GPa (Aluminum) to 200 GPa (stainless steel), which also can broaden the force and torque ranges dramatically. All the measures mentioned above can be completed conveniently and easily. Therefore, the TTS can be used in practical industrial environments without considering the detecting range problem.

Self-decoupling is a unique, excellent characteristic of the proposed TTS. Fig.10 and Fig.11 together prove that the TTS has a good self-decoupling ability. No decoupling algorithm is needed in TTS, which decreases the decoupling complication.

Passive ability means that the TTS can work for an unlimited time without replenishing the energy or replacing the batteries. Here, we would like to give a more exact definition of the concept ''Passive.'' The concept ''passive'' refers to an absence of batteries or wires on the sensor itself to provide power. However, the affiliated detecting apparatus is not in the ''passive'' scope [25], [26]. The proposed TTS does not need wires or batteries to provide energy; benefiting from the Villari effect, the working energy needed by the TTS can be provided by a spatial magnetic field, which achieves the passive detection of the TTS. The signals reflecting the force and torque can also be transmitted through the spatial magnetic field. No wires are needed for power supply and signal transmission, which is very different from the traditional resistance strain gauges [27], optoelectronic sensors [18], piezoelectric sensors [20], and the like. Furthermore, the TTS can rotate with the external payload without wire problems. Thus, our TTS provides a new way to detect coupled force and torque passively and wirelessly. Fig.12 and Fig.13 both demonstrate the passive characteristcs of TTS.

Working dynamically is much more difficult to realize for some common multi-dimensional sensors such as the resistance or optoelectronic sensors [18], [27], [28]. The wires of these sensors keep them from rotating continuously. However, the specially designed TTS in this article can realize dynamic detection, which is verified by Fig. 12 and Fig.13. In the two Figures, rotating velocities have almost no influence on the signal output of the sensor. Fig.12 and Fig.13 together demonstrate the dynamic working ability of the TTS.

The drift and hysteretic characteristics are fundamental characteristics of a sensor. Fig.14 demonstrates that the drifts of the tension force detecting voltage and the torque detecting voltage are very small, which indicates that TTS has a stable output. Fig.15 shows that the hysteresis between the forward and the backward curves was small. Thus, the TTS has a good output performance. Fig.14 and Fig.15 together prove that the TTS is reasonably designed, properly fabricated, and works effectively.

Working in a liquid envriomentdynamically is a superiority of the proposed TTS [7], [29]. Fig.16 proves that the TTS can work in a liquid environment. In the TTS design, the power supply and the signal transmission are fulfilled by a magnetic field, which is a unique property compared to traditional wires, for the magnetic field can pass the liquid easily. The magnetic field allows the TTS to work easily in the water. The voltage output in the water is similar to that in the air, except the voltage increments. The pemeability of air is larger than the pemeability of water. Therefore, the voltage in air is larger than that in water, which explains why the voltage increment in air is larger than that in water. In practrical applications, voltage output can be calibrated in the target liquid to acquire a special relationship. Working in a liquid environment gives the TTS the potential for application in a rigorous liquid environment, such as in milling cutters surrounded by cutting fluid.

TABLE 2. Comparison between our TTS and those in previous works.

Items	The proposed TTS	The sensor in [15]	The sensor in [30]	The sensor in [23]
Force types	Tension and Torque	Torque only	Torque only	Tension and Torque
Sensing range	1000 N and 6.5 N·m	Determined by diameter	Determined by diameter	40 N and 4 N·m
Stability	Good	Moderate	Moderate	Poor
Decoupling method	self-decoupled	Not applicable	Not applicable	Algorithm decoupled
Power supply	Passive	Passive	Battery	Passive
Ability to work in liquid	Yes	No	No	Yes

All the advantages listed above demonstrate that the TTS is an innovatively designed force and torque sensor. The self-decoupled and passive TTS was compared with several force sensors, as shown in Table 2. The items of force types, sensing range, stability, decoupling method, power supply, and ability to work in liquid were compared. From the comparison, the proposed TTS had a very good superiority with

regard to the items of the decoupling method, power supply, and ability to work in liquid. These merits enable the proposed TTS to work passively, wirelessly, and dynamically. Thus, the TTS can potentially work in a liquid and rotating environment.

V. CONCLUSION

A self-decoupled and passive sensor for dynamically detecting force and torque was proposed, called the TTS, which can decouple the compound force and torque through a T-type mechanical structure. The rotating speed has no influence on the TTS, and the TTS can work in a rotating environment. The maximum voltage fluctuation caused by the rotation movement is 0.05 mV, and the drift and hysteresis characteristics of the TTS are very good. Furthermore, the TTS can work freely in a liquid environment. Compared with previous force sensors, the TTS has the advantages of being self-decoupled and passive, and the ability to work dynamically and in a liquid environment. All of these merits make the TTS potentially useful in multi-dimensional, dynamic, and liquid environments. The focus of our future research will be to develop a self-decoupled and passive sensor with more than two dimensions.

REFERENCES

[1] A. Song, J. Wu, G. Qin, and W. Huang, "A novel self-decoupled four degree-of-freedom wrist force/torque sensor," *Measurement*, vol. 40, nos. 9–10, pp. 883–891, Nov. 2007.
[2] S. Chen, J. Wang, and P. Kazanzides, "Integration of a low-cost three-axis sensor for robot force control," in *Proc. 2nd IEEE Int. Conf. Robotic Comput. (IRC)*, Jan. 2018, pp. 246–249.
[3] M.-K. Kang, S. Lee, and J.-H. Kim, "Shape optimization of a mechanically decoupled six-axis force/torque sensor," *Sens. Actuators A, Phys.*, vol. 209, pp. 41–51, Mar. 2014.
[4] J. B. Gafford, S. B. Kesner, A. Degirmenci, R. J. Wood, R. D. Howe, and C. J. Walsh, "A monolithic approach to fabricating low-cost, millimeter-scale multi-axis force sensors for minimally-invasive surgery," in *Proc. IEEE Int. Conf. Robot. Autom. (ICRA)*, May 2014, pp. 1419–1425.
[5] Q. Liang, D. Zhang, Y. Wang, and Y. Ge, "Development of a touch probe based on five-dimensional force/torque transducer for coordinate measuring machine (CMM)," *Robot. Comput.-Integr. Manuf.*, vol. 28, no. 2, pp. 238–244, Apr. 2012.
[6] Y. Tan, X. Wang, and L. Ren, "Design and experiment of a cardan-type self-decoupled and self-powered bending moment and torque sensor," *IEEE Trans. Ind. Electron.*, early access, May 7, 2020, doi: 10.1109/TIE.2020.2991931.
[7] Q. Liang, D. Zhang, Q. Song, and Y. Ge, "A potential 4-D fingertip force sensor for an underwater robot manipulator," *IEEE J. Ocean. Eng.*, vol. 35, no. 3, pp. 574–583, Jul. 2010.
[8] L.-P. Chao and K.-T. Chen, "Shape optimal design and force sensitivity evaluation of six-axis force sensors," *Sens. Actuators A, Phys.*, vol. 63, no. 2, pp. 105–112, Oct. 1997.
[9] T. A. Dwarakanath, B. Dasgupta, and T. S. Mruthyunjaya, "Design and development of a stewart platform based force–torque sensor," *Mechatronics*, vol. 11, no. 7, pp. 793–809, Oct. 2001.
[10] Y. Lu, Y. Wang, N. Ye, and L. Chen, "Development of a novel sensor for hybrid hand with three fingers and analysis of its measure performances," *Mech. Syst. Signal Process.*, vol. 83, pp. 116–129, Jan. 2017.
[11] G. Mastinu, M. Gobbi, and G. Previati, "A new six-axis load Cell. Part I: Design," *Experim. Mech.*, vol. 51, no. 3, pp. 373–388, Mar. 2011.
[12] A. Mura, "Six d.O.f. displacement measuring device based on a modified stewart platform," *Mechatronics*, vol. 21, no. 8, pp. 1309–1316, Dec. 2011.
[13] Y. Hayashi, N. Tsujiuchi, T. Koizumi, H. Oshima, A. Ito, and Y. Tsuchiya, "Optimum design of the thin-type four-axis force/moment sensor for a robot finger," in *Proc. 36th Annu. Conf. IEEE Ind. Electron. Soc.*, Nov. 2010, pp. 1287–1292.
[14] L. Feng, W. Chen, T. Wu, H. Wang, D. Dai, D. Wang, and W. Zhang, "An improved sensor system for wheel force detection with motion-force decoupling technique," *Measurement*, vol. 119, pp. 205–217, Apr. 2018.
[15] J. K. Lee, H. M. Seung, C. I. Park, J. K. Lee, D. H. Lim, and Y. Y. Kim, "Magnetostrictive patch sensor system for battery-less real-time measurement of torsional vibrations of rotating shafts," *J. Sound Vib.*, vol. 414, pp. 245–258, Feb. 2018.
[16] L. Zhao, J. Chen, T. Chen, Y. Shi, Z. Fan, and Z. Zhuang, "Zero-voltage and zero-current switching Dual-Transformer-Based full-bridge converter with current doubler rectifier," *IEEE Trans. Power Electron.*, vol. 35, no. 12, pp. 12949–12958, Dec. 2020, doi: 10.1109/TPEL.2020.2997017.
[17] J. Chen, H. Shao, Y. Cheng, X. Wang, G. Li, C. Sun, Q. Jiang, and J. Qin, "Harmonic circulation and DC voltage instability mechanism of parallel-SVG system," *IET Renew. Power Gener.*, vol. 14, no. 5, pp. 793–802, Apr. 2020.
[18] G. Palli, L. Moriello, U. Scarcia, and C. Melchiorri, "Development of an optoelectronic 6-axis force/torque sensor for robotic applications," *Sens. Actuators A, Phys.*, vol. 220, pp. 333–346, Dec. 2014.
[19] L. Xiong, G. Jiang, Y. Guo, and H. Liu, "A three-dimensional fiber Bragg grating force sensor for robot," *IEEE Sensors J.*, vol. 18, no. 9, pp. 3632–3639, May 2018.
[20] Y.-J. Li, C. Yang, G.-C. Wang, H. Zhang, H.-Y. Cui, and Y.-L. Zhang, "Research on the parallel load sharing principle of a novel self-decoupled piezoelectric six-dimensional force sensor," *ISA Trans.*, vol. 70, pp. 447–457, Sep. 2017.
[21] M. N. Ul Islam, P. Cheng, and B. Oelmann, "Torque sensor design considering thermal stability for harsh industrial environments," in *Proc. 12th Int. Conf. Sens. Technol. (ICST)*, Dec. 2018, pp. 83–86.
[22] L. M. Reindl, "Wireless passive sensors: Basic principles and performances," in *Proc. IEEE Sensors*, Dec. 2008, pp. 1607–1610.
[23] Y. Tan, J. Zhu, and L. Ren, "A Two-Dimensional Wireless and Passive Sensor for Stress Monitoring," *Sensors*, vol. 19, no. 1, pp. 135–147, Jan. 2019.
[24] A. Viola, V. Franzitta, G. Cipriani, V. Di Dio, F. M. Raimondi, and M. Trapanese, "A magnetostrictive electric power generator for energy harvesting from traffic: Design and experimental verification," *IEEE Trans. Magn.*, vol. 115, no. 11, pp. 2–5, 2015.
[25] Y. Tan, G. Lu, M. Cong, X. Wang, and L. Ren, "Gathering energy from ultra-low-frequency human walking using a double-frequency up-conversion harvester in public squares," *Energy Convers. Manag.*, vol. 217, no. 5, pp. 112958–112966, 2020.
[26] Y. Tan, Y. Zhang, and L. Ren, "Energy harvesting from an artificial bone," *IEEE Access*, vol. 7, pp. 120065–120075, 2019.
[27] Q. Liang, D. Zhang, Q. Song, Y. Ge, H. Cao, and Y. Ge, "Design and fabrication of a six-dimensional wrist force/torque sensor based on E-type membranes compared to cross beams," *Measurement*, vol. 43, no. 10, pp. 1702–1719, Dec. 2010.
[28] T. A. Dwarakanath and G. Bhutani, "Beam type hexapod structure based six component force–torque sensor," *Mechatronics*, vol. 21, no. 8, pp. 1279–1287, Dec. 2011.
[29] M. R. Arshad, "Recent advancement in sensor technology for underwater applications," *Indian J. Marine Sci.*, vol. 38, no. 3, pp. 267–273, 2009.
[30] Y. Fan, P. Kong, H. Qi, H. Liu, and X. Ji, "A surface acoustic wave response detection method for passive wireless torque sensor," *AIP Adv.*, vol. 8, no. 1, pp. 1–12, 2018.

YISONG TAN (Member, IEEE) was born in Shandong, China, in 1982. He received the B.S. degree from the School of Mechanical Engineering, Shandong University, China, in 2005, and the M.S. and Ph.D. degrees from the School of Mechatronics Engineering, Harbin Institute of Technology, China, in 2007 and 2012, respectively. He joined the School of Mechanical Engineering, Northeast Electric Power University, China, in 2012. He is currently an Associate Professor with Northeast Electric Power University. His research interests include multidimensional sensor, magnetostrictive sensors, and human motion energy harvesting.

YIFU FU was born in Jilin, China, in 1994. He received the B.S. degree from the School of Mechanical Engineering, Northeast Electric Power University, China, in 2017, where he is currently pursuing the M.S. degree. His research interest includes multidimensional sensor.

XINYU WANG was born in Jilin, China, in 1994. He received the B.S. degree from the School of Mechanical Engineering, Northeast Electric Power University, China, in 2017, where he is currently pursuing the M.S. degree. His research interest includes magnetostrictive sensor.

MOYUE CONG was born in Shandong, China, in 1993. He received the B.S. degree from the School of Mechanical Engineering, Northeast Electric Power University, China, in 2017, where he is currently pursuing the M.S. degree. His research interest includes magnetostrictive sensor.

LIMIN REN (Member, IEEE) was born in Heilongjiang, China, in 1982. She received the B.S. degree from the School of Mechanical Engineering, Heilongjiang Bayi Agricultural University, China, in 2004, and the M.S. and Ph.D. degrees from the School of Mechatronics Engineering, Harbin Institute of Technology, China, in 2007 and 2012, respectively. She joined the School of Mechanical Engineering, Northeast Electric Power University, China, in 2014. She is currently an Associate Professor with Northeast Electric Power University. Her research interests include multidimensional sensor, magnetostrictive sensors, and human motion energy harvesting.